Intrinsic and extrinsic diffusion of indium in germanium

Journal Item

Intrinsic and extrinsic diffusion of indium in germanium

R. Kube,[1] H. Bracht,[1,a)] A. Chroneos,[2] M. Posselt,[3] and B. Schmidt[3]
[1]*Institute of Material Physics, University of Münster, Wilhelm-Klemm-Straße 10, D-48149 Münster, Germany*
[2]*Department of Materials, Imperial College London, London SW7 2BP, United Kingdom*
[3]*Institute of Ion Beam Physics and Materials Research, Forschungszentrum Dresden-Rossendorf, D-01314 Dresden, Germany*

(Received 11 August 2009; accepted 21 August 2009; published online 28 September 2009)

Diffusion experiments with indium (In) in germanium (Ge) were performed in the temperature range between 550 and 900 °C. Intrinsic and extrinsic doping levels were achieved by utilizing various implantation doses. Indium concentration profiles were recorded by means of secondary ion mass spectrometry and spreading resistance profiling. The observed concentration independent diffusion profiles are accurately described based on the vacancy mechanism with a singly negatively charged mobile In-vacancy complex. In accord with the experiment, the diffusion model predicts an effective In diffusion coefficient under extrinsic conditions that is a factor of 2 higher than under intrinsic conditions. The temperature dependence of intrinsic In diffusion yields an activation enthalpy of 3.51 eV and confirms earlier results of Dorner *et al.* [Z. Metallk. **73**, 325 (1982)]. The value clearly exceeds the activation enthalpy of Ge self-diffusion and indicates that the attractive interaction between In and a vacancy does not extend to third nearest neighbor sites which confirms recent theoretical calculations. At low temperatures and high doping levels, the In profiles show an extended tail that could reflect an enhanced diffusion at the beginning of the annealing.

[doi:10.1063/1.3226860]

I. INTRODUCTION

The elemental semiconductor Ge has received renewed interest due to its potential use in the fabrication of complementary metal oxide semiconductors (CMOSs). By utilizing Ge instead of silicon (Si) for CMOS technology, one can take advantage of the higher electron and hole mobilities in Ge compared to Si.[1] Whereas a *p*-channel Ge-MOSFET made of heavily boron (B) doped source and drain regions have already been demonstrated,[2,3] the *n*-channel MOSFET remains a challenge due to the enhanced diffusion of *n*-type dopants under extrinsic doping conditions and the deactivation of the donors for concentrations exceeding 10^{19} cm^{-3}.[3–7] The enhanced diffusion and deactivation are directly associated with the properties of the point defects involved in the diffusion mechanisms.[6,7] In the case of phosphorus (P), arsenic (As), and antimony (Sb) diffusion in Ge, the mass transport is mediated by singly negatively charged donor-vacancy pairs.[6] The charge difference between the mobile pair and the substitutional donor, that is singly positively charged, leads to a donor diffusion coefficient proportional to the square of the free electron concentration.[6] The physical origin of this concentration enhanced diffusion of *n*-type dopants under extrinsic doping conditions is the electric field established by the donor atoms that leads to a drift of the donor-vacancy pairs.[8] As far as technological requirements are considered, B in Ge behaves almost diffusionless[9] and high activation levels can be achieved after annealing B-implanted preamorphized Ge.[10,11] The low B diffusion, which is associated with a diffusion activation enthalpy exceeding the value of Ge self-diffusion,[9] can be explained with both the vacancy and interstitialcy mechanisms. In the case vacancies (V) mediate B diffusion, the high activation enthalpy reflects a repulsive interaction between B and V due to, e.g., local stress and/or the charge states of the point defects involved in the defect reaction. The repulsive interaction of the BV pair has been recently verified by density functional theory (DFT) calculations.[12] In the case when the interstitialcy mechanism mediates B diffusion, the high activation enthalpy would support a high enthalpy for the formation of self-interstitials that agrees with theoretical predictions.[13–16] According to previous studies on the diffusion of other acceptor dopants such as aluminum (Al),[17] gallium (Ga),[18,19] and In,[20] these elements diffuse several orders of magnitude faster than B.[5] The diffusion experiments reported by Dorner *et al.*,[17,20] Södervall *et al.*,[18] and Riihimäki *et al.*[19] yield diffusion activation enthalpies for Al, Ga, and In that clearly exceed the activation enthalpy of self-diffusion.[21,22] Considering the DFT calculations of Chroneos *et al.*,[23,24] these results seem to be in conflict with the picture on a vacancy-mediated acceptor diffusion that predict diffusion activation enthalpies below 3 eV for Al, Ga, and In. In order to verify the diffusion activation enthalpy, we report in this paper experiments on the intrinsic and extrinsic diffusion of In in Ge. In contrast to the strong concentration dependent diffusion of donor atoms in Ge, the diffusion of In is independent of the acceptor concentration indicating that the charge state of the mobile InV pair equals that of substitutional In (In_s^-). However, an effective In diffusion coefficient is obtained from an analytical analysis of

a)Author to whom correspondence should be addressed. Electronic mail: bracht@uni-muenster.de.

extrinsic In profiles that can be at most a factor of 2 higher than In diffusion under intrinsic conditions. The analysis of acceptor diffusion presented in this work will help to understand in more detail the diffusion behavior of *p*-type dopants in Ge under intrinsic and extrinsic conditions and, in particular, serves to differentiate between the diffusion coefficients deduced from a simple analytical and a more comprehensive numerical analysis of experimental profiles.

II. EXPERIMENTAL

(100)-oriented high Ohmic (>30 Ω cm) *p*-type single crystalline Ge wafers with a thickness of about 500 μm were used for the diffusion experiments. The wafers were provided by Umicore (Olen, Belgium). Two samples with lateral dimensions of 10×10 and 17×24 mm^2 were cut and implanted with In at 350 keV. One of the samples was implanted with an In dose of 1.1×10^{14} cm^{-2} and the other with 1.1×10^{15} cm^{-2} resulting in In-peak concentrations of 10^{19} and 10^{20} cm^{-3}, respectively. Subsequently, the In-implanted samples were cut into smaller pieces, cleaned with organic solvents, hydrofluoric acid, and de-ionized water, and encapsulated in evacuated quartz ampoules. Additionally, we also prepared Ge samples that were covered on one side with high purity In (99.9999%) by means of vacuum evaporation. Diffusion annealing were performed at temperatures between 550 and 900 °C for various times in a resistance heated furnace. A type-S, Pt–PtRh, thermocouple was used to monitor the temperature with an accuracy of ±2 K. The ampoules were quenched in ethylene glycol to terminate the diffusion process. Time of flight secondary ion mass spectrometry (TOF-SIMS 5) at TASCON GmbH (Münster) was applied to determine the distribution of In in the as-implanted and annealed Ge samples. The as-implanted profiles were used as reference samples for the calibration of the SIMS profiles. The depths of the craters that are formed by the SIMS analysis were determined with an optical profilometer NT3300 at Nanoanalytics (Münster). For the highest diffusion temperature, we used In-evaporated Ge samples and applied the spreading resistance technique for profiling. For the conversion of the spreading resistance profiles to resistivity profiles, we used homogenously doped reference samples of known resistivities. Conversion of the resistivity data to dopant concentrations is based on the interrelation between the acceptor concentration and the respective resistivity reported by Cuttriss.[25]

III. RESULTS

Typical concentration profiles of In measured with TOF-SIMS after diffusion annealing of low- and high-dose In-implanted Ge samples at 700 °C for 24 h are illustrated in Fig. 1. The lower profile with a maximum concentration of about 10^{18} cm^{-3} reflects the diffusion behavior of In in Ge under intrinsic conditions ($p/n_i\approx1$). The upper In profile with a maximum concentration of 10^{19} cm^{-3} is representative for extrinsic diffusion ($p/n_i>1$). The shape of the intrinsic profile that exhibits a lower In concentration close to the surface compared to the bulk suggests that during annealing In leaves the Ge sample; i.e., the Ge surface acts as sink.

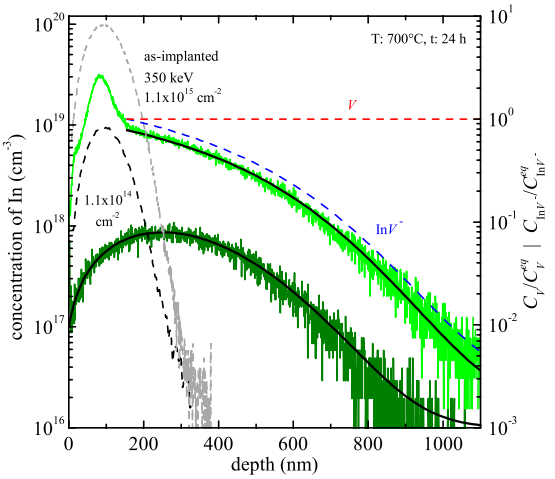

FIG. 1. (Color online) Indium concentration profiles measured with TOF-SIMS after diffusion annealing of the low- and high-dose In-implanted Ge samples (lower and upper solid lines, respectively) at the temperature and time indicated. The low- and high-doses as-implanted In profiles are illustrated by the lower and upper dashed lines. The implantation energy and doses are indicated. The black solid lines are simulations of In diffusion performed based on reaction (2). The corresponding distribution of vacancies and In-vacancy pairs are displayed by the dashed lines that refer to the right *y*-axis.

In contrast, the upper extrinsic profile reveals an immobile In peak with a concentration exceeding 10^{19} cm^{-3} close to the surface. Following atomistic calculations on the stability of In_nV_m clusters, it is very likely that such clusters mainly exist in the high concentration region.[26] During annealing, these clusters dissolve and act as source for mobile In-related defects that penetrate into the bulk and transform to substitutional In. Other profiles representing intrinsic and extrinsic diffusion are displayed in Figs. 2 and 3, respectively. Figure 4 shows In profiles measured by means of the spreading resistance technique. The diffusion temperature *T* and time *t* as well as maximum In concentration of all analyzed samples

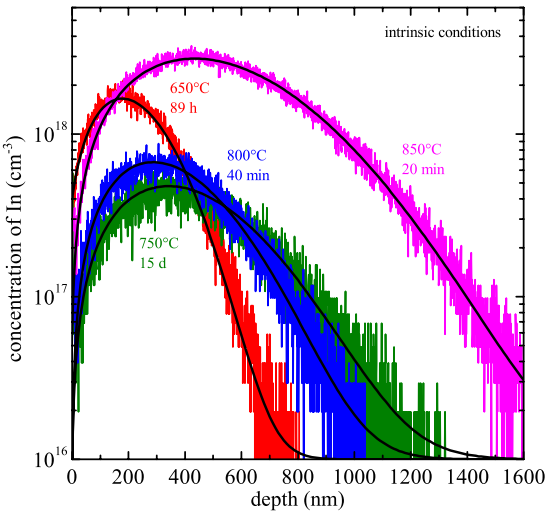

FIG. 2. (Color online) Indium concentration profiles in Ge measured with TOF-SIMS after diffusion annealing at the temperatures and times indicated. All profiles refer to intrinsic diffusion conditions that are established during annealing of the low-dose In-implanted Ge samples. The solid lines represent numerical simulations based on reaction (2) with an In sink at the surface.

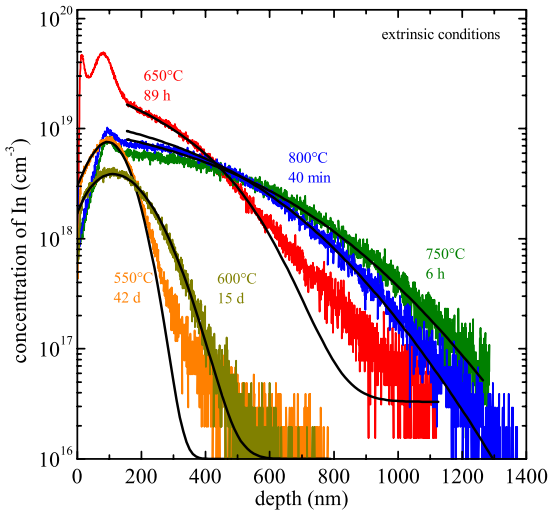

FIG. 3. (Color online) Indium concentration profiles in Ge measured with TOF-SIMS after diffusion annealing at the temperatures and times indicated. All profiles refer to extrinsic diffusion conditions that are established during annealing of the low-dose In-implanted Ge samples at 550 and 600 °C and during annealing of the high-dose In-implanted samples at higher temperatures. The solid lines represent numerical simulations based on reaction (2) assuming an In sink at the surface for 550 and 600 °C and an infinite In source at about 150 nm beneath the surface for the higher temperatures.

are listed in Table I. This table also comprises the intrinsic carrier concentration n_i at the respective temperatures according to Eq. (6) of Ref. 6 and the ratio p/n_i as a measure of the electronic condition established during annealing.

IV. ANALYSIS

A. Fitting of experimental profiles

The experimental In profiles resemble in shape a complementary error function (upper profile of Fig. 1) or a Gaussian profile (lower profile of Fig. 1) that represent the solutions of Fick's second law of diffusion for a concentration independent diffusion coefficient with infinite and finite dopant sources, respectively. Therefore, in order to deduce the diffusion coefficient of In in Ge, we first consider, for simplicity, Fick's second law of diffusion:

$$\frac{\partial C_{\mathrm{In}}(x,t)}{\partial t} = D_{\mathrm{In}}^{\mathrm{eff}} \frac{\partial^2 C_{\mathrm{In}}(x,t)}{\partial x^2}, \tag{1}$$

where C_{In} represents the concentration of In and $D_{\mathrm{In}}^{\mathrm{eff}}$ represents an effective diffusion coefficient. In the case of intrinsic diffusion, the low-dose as-implanted In profile is considered as initial profile for $t=0$ s. The surface is assumed to act as sink. This is reflected by the strong gradient in the In concentration close to the Ge surface (see lower profile of Fig. 1 and the profiles of Fig. 2). Taking into account these initial and boundary conditions, the differential equation (1) is solved numerically. The solution accurately describes the experimental profiles for intrinsic conditions (not shown in Figs. 1 and 2). The effective diffusion coefficients $D_{\mathrm{In}}^{\mathrm{eff}}$ deduced from this analysis are given in Table I. In the case of extrinsic diffusion, the In peak observed in Figs. 1 and 3 at about 100 nm beneath the surface is considered to act as In source during annealing. At about 150 nm beneath the surface, a crossover from the peak to the profile is observed. At this point, we assume a constant concentration of In to be maintained by the In clusters in the peak region. Taking into account this boundary concentration, the solution of Eq. (1) is given by a complementary error function. Fitting this function to the experimental extrinsic In profiles provides accurate fits (not shown in Fig. 3) with values for $D_{\mathrm{In}}^{\mathrm{eff}}$ listed in Table I. The extrinsic In profiles obtained after diffusion annealing at 550 and 600 °C do not reveal a crossover from the peak to the profile (see Fig. 3). These profiles were fitted by solving Eq. (1) numerically assuming the as-implanted In profile as initial profile and an In sink at the surface. Comparison of the effective diffusion coefficients $D_{\mathrm{In}}^{\mathrm{eff}}$ for intrinsic and extrinsic conditions reveals data for extrinsic conditions that are about a factor of 2 higher than the data for intrinsic conditions. This is, e.g., confirmed by the profiles obtained after diffusion annealing at 650, 700, 750, and 800 °C. The In profiles illustrated in Fig. 4, which were recorded with the spreading resistance technique after annealing Ge samples with an evaporated In layer on top of the surface, all represent intrinsic diffusion conditions $p/n_i \approx 1$ (see Table I). The profile for 880 °C is best reproduced with a complementary error function indicating an infinitive In source at the surface. The profiles for 850 and 900 °C are best described with a Gaussian profile indicating a finite In source. The data obtained in this way for $D_{\mathrm{In}}^{\mathrm{eff}}$ are listed in Table I. The origin of the different effectiveness of In at the surface is probably related to different thicknesses of the evaporated In layers. Thin layers likely serve as finite and thick layers as infinite In source.

A difference in $D_{\mathrm{In}}^{\mathrm{eff}}$ for intrinsic and extrinsic conditions is predicted by the vacancy mechanism when the following reaction is assumed:[8]

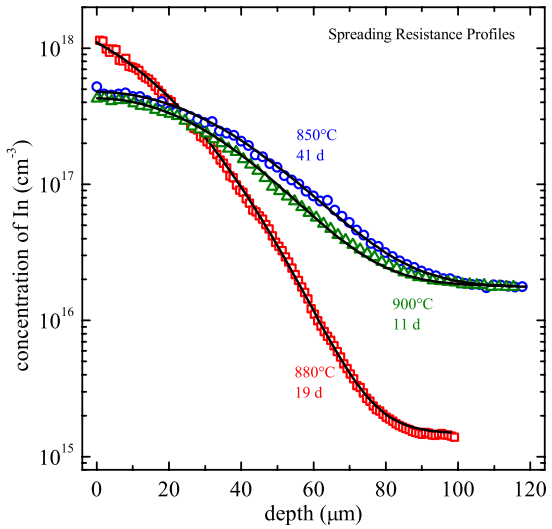

FIG. 4. (Color online) Indium concentration profiles in Ge measured by means of spreading resistance profiling after diffusion annealing at the temperatures and times indicated. The profiles refer to intrinsic diffusion conditions and are accurately described with a complementary error function (black solid line for 880 °C) and a Gaussian profile (black solid lines for 850 and 900 °C) that, respectively, represent an infinitive and a finite In-evaporated layer on top of the surface.

TABLE I. Intrinsic diffusion coefficient $D_{\mathrm{In}}(n_i)[\equiv D^*_{\mathrm{In}}]$ of indium in germanium determined from modeling the intrinsic and extrinsic diffusion profiles shown in Figs. 1–4. The effective diffusion coefficient $D^{\mathrm{eff}}_{\mathrm{In}}$ is obtained in the case Fick's second law of diffusion is considered for the diffusion analysis. $D^{\mathrm{eff}}_{\mathrm{In}}$ can deviate by at most a factor of 2 from the reduced diffusion coefficient D^*_{In} that is determined when the full differential equation system representing In diffusion via reaction (2) is considered. Also listed are the corresponding diffusion temperature T and time t, maximum dopant concentration $C^{\mathrm{eq}}_{\mathrm{In}}$, maximum hole concentration $p=0.5[C^{\mathrm{eq}}_{\mathrm{In}}+\sqrt{(C^{\mathrm{eq}}_{\mathrm{In}})^2+4n_i^2}]$, and intrinsic carrier concentration n_i.

T (°C)	t (s)	$C^{\mathrm{eq}}_{\mathrm{In}}$ (cm^{-3})	n_i (cm^{-3})	p (cm^{-3})	p/n_i	$D^{\mathrm{eff}}_{\mathrm{In}}$ (cm^2/s)	D^*_{In} (cm^2/s)
550	3 607 200	8.0×10^{18}	1.5×10^{18}	8.3×10^{18}	5.6	2.0×10^{-18}	1.1×10^{-18}
600	1 296 000	4.0×10^{18}	2.1×10^{18}	4.9×10^{18}	2.3	3.9×10^{-17}	2.5×10^{-17}
650	320 400	1.8×10^{18}	2.9×10^{18}	3.9×10^{18}	1.4	4.8×10^{-16}	4.7×10^{-16}
650	320 400	1.7×10^{19}	2.9×10^{18}	1.7×10^{19}	5.9	9.4×10^{-16}	5.6×10^{-16}
700	86 400	8.8×10^{17}	3.8×10^{18}	4.3×10^{18}	1.1	3.4×10^{-15}	3.4×10^{-15}
700	86 400	9.4×10^{18}	3.8×10^{18}	1.1×10^{19}	2.8	6.8×10^{-15}	5.0×10^{-15}
750	22 200	4.4×10^{17}	5.0×10^{18}	5.2×10^{18}	1.1	2.4×10^{-14}	2.5×10^{-14}
750	21 600	8.0×10^{18}	5.0×10^{18}	1.0×10^{19}	2.1	4.0×10^{-14}	3.4×10^{-14}
800	2 400	6.8×10^{17}	6.3×10^{18}	6.6×10^{18}	1.1	1.6×10^{-13}	1.6×10^{-13}
800	2 400	9.5×10^{18}	6.3×10^{18}	1.3×10^{19}	2.0	2.7×10^{-13}	2.3×10^{-13}
850[a]	1 200	3.1×10^{17}	7.7×10^{18}	7.9×10^{18}	1.0	7.2×10^{-13}	7.4×10^{-13}
850	1 200	3.2×10^{18}	7.7×10^{18}	9.5×10^{18}	1.2	7.6×10^{-13}	7.7×10^{-13}
850	3 542 400	5.2×10^{17}	7.7×10^{18}	8.0×10^{18}	1.0	1.3×10^{-12}	1.3×10^{-12}
880	1 641 600	1.1×10^{18}	8.7×10^{18}	9.3×10^{18}	1.1	1.6×10^{-12}	1.7×10^{-12}
900	950 400	3.7×10^{17}	9.4×10^{18}	9.6×10^{18}	1.0	4.1×10^{-12}	4.1×10^{-12}

[a]The corresponding In profile is not shown in Fig. 2 for clarity.

$$(\mathrm{In}V)^- \leftrightarrow \mathrm{In}_s^- + V^0, \tag{2}$$

where $(\mathrm{In}V)^-$ and In_s^- represent the In-vacancy pair and the substitutional In, respectively. Both defects are singly negatively charged. V^0 denotes a neutral vacancy. Indium diffusion via reaction (2) is described by three coupled partial differential equations.[8] Numerical simulations taking into account the full differential equation system are illustrated by the black solid lines in Figs. 1–3. The parameter values for D^*_{In} that best reproduce the extrinsic and intrinsic profiles are listed in Table I. The values for D^*_{In} deduced from intrinsic and extrinsic profiles at a given temperature are equal within the experimental accuracy of 20% showing that In diffusion in Ge is independent of the acceptor concentration. However, a comparison to the data of $D^{\mathrm{eff}}_{\mathrm{In}}$ indicates that with increasing p/n_i, the ratio $D^{\mathrm{eff}}_{\mathrm{In}}/D^*_{\mathrm{In}}$ approaches 2 as illustrated in Fig. 5. This interrelation between $D^{\mathrm{eff}}_{\mathrm{In}}$ and D^*_{In} is fully explained based on reaction (2). In the foreign-atom controlled mode of extrinsic diffusion, i.e., when $C^{\mathrm{eq}}_{\mathrm{In}V^-}D_{\mathrm{In}V^-} \ll C^{\mathrm{eq}}_V D_V$, $C_V(x,t) \approx C^{\mathrm{eq}}_V$, and $p \approx C^{\mathrm{eq}}_{\mathrm{In}_s^-}$ hold, the full differential equation system can be reduced to Eq. (1) with an effective, concentration independent diffusion coefficient given by $D^{\mathrm{eff}}_{\mathrm{In}}=2D^*_{\mathrm{In}}$ and $D^*_{\mathrm{In}}=C^{\mathrm{eq}}_{\mathrm{In}V^-}D_{\mathrm{In}V^-}/C^{\mathrm{eq}}_{\mathrm{In}}$ [see Eq. (48) of Ref. 8]. Thus the experimentally determined interrelation between intrinsic and extrinsic diffusion of In in Ge proves that the charge state of the mobile InV pair must be equal to the charge state of substitutional In; i.e., both are singly negatively charged. In the case the charge states of InV and In_s were different, the extrinsic diffusion of In should be dependent on the In acceptor concentration which is not verified by the experiments.

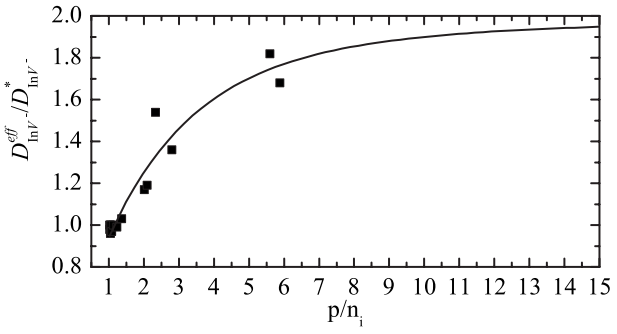

FIG. 5. Ratio $D^{\mathrm{eff}}_{\mathrm{In}}/D^*_{\mathrm{In}}$ vs the reduced hole concentration p/n_i. With increasing doping level, the difference between the effective and reduced diffusion coefficients $D^{\mathrm{eff}}_{\mathrm{In}}$ and D^*_{In} approaches the factor of 2. Under intrinsic conditions $D^{\mathrm{eff}}_{\mathrm{In}}=D^*_{\mathrm{In}}$ and under extrinsic conditions, reaction (2) predicts $D^{\mathrm{eff}}_{\mathrm{In}}=2D^*_{\mathrm{In}}$ (see text for details). The solid line serves to guide the eye.

The analysis of In diffusion based on Fick's second law [see Eq. (1)] and on the full differential equation system representing reaction (2) yields in the former case the effective diffusion coefficient $D^{\mathrm{eff}}_{\mathrm{In}}$ and in the later case the reduced diffusion coefficient D^*_{In}. Under intrinsic diffusion conditions, $D^{\mathrm{eff}}_{\mathrm{In}}$ equals D^*_{In} but under extrinsic conditions the relation $D^{\mathrm{eff}}_{\mathrm{In}}=2D^*_{\mathrm{In}}$ holds. The ratio $D^{\mathrm{eff}}_{\mathrm{In}}/D^*_{\mathrm{In}}$ as function of the hole concentration p normalized by the intrinsic carrier concentration n_i is equal to 1 for intrinsic doping and approaches 2 for high doping levels (see Fig. 5). This interrelation between $D^{\mathrm{eff}}_{\mathrm{In}}$ and D^*_{In} demonstrates that the diffusion coefficient may not represent intrinsic conditions even in the case when dopant diffusion under extrinsic condition is independent of the acceptor concentration.

B. Motivation of diffusion model and numerical simulations

Diffusion experiments under equilibrium conditions are hardly sensitive to the nature of the point defects involved in the defect reactions.[8] Accordingly, In diffusion in Ge, in prin-

ciple, cannot provide the information that vacancies mediate the diffusion as this is suggested by reaction (2). However, vacancies are generally considered to prevail in Ge under thermal equilibrium conditions. This has been concluded from self- and foreign-atom diffusion studies[7,21,22,27–30] and confirmed by atomistic calculations.[15,23,30–33] In particular, the simultaneous diffusion of self- and dopant atoms in isotopically controlled Ge heterostructures have revealed that vacancies in Ge are mainly doubly negatively charged under intrinsic and *n*-type doping conditions.[7,34] However, the preferred charge state of *V* under *p*-type doping is not known. In line with these findings that vacancies in Ge dominate atomic transport under thermal equilibrium conditions, we also assume that the diffusion of In is mediated by *V*. Whereas the charge state of the mobile In-related defect, i.e., of the In*V* pair, can be determined, the charge state of the vacancy cannot be deduced from In diffusion because the foreign-atom controlled diffusion mode is established. In this mode the concentration of vacancies is close to their thermal equilibrium and the calculated In profiles are insensitive to the charge state of the vacancy and the individual settings of the equilibrium concentration C_V^{eq} and diffusion coefficient D_V as long as the relationship $C_{InV^-}^{eq} D_{InV^-} \ll C_V^{eq} D_V$ is preserved. For modeling, we used values for $C_V^{eq} D_V$ determined from the Ge self-diffusion coefficient $D_{Ge} = 0.5 C_V^{eq} D_V / C_o$, where $C_o (=4.413 \times 10^{22}\ \mathrm{cm}^{-3})$ is the Ge atom density. These values represent the upper bounds of Ge self-diffusion under *p*-type doping. Since the vacancy is doubly negatively charged in Ge under intrinsic conditions,[7,34] Ge self-diffusion should be retarded with increasing *p*-type doping. The concentration of the In*V* pairs and vacancies was considered to be three and five orders of magnitude lower than the concentration of substitutional In, respectively. The simulations are fairly insensitive to the equilibrium concentration of In*V* pairs since for a mainly substitutionally dissolved dopant the concentration of In*V* will certainly not exceed the concentration of substitutional In. Lattice location studies of implanted In in Ge show that the major fraction of In is located on substitutional site and evidence on the formation of In*V* pairs are found.[35–42] Altogether, as far as atomic diffusion is concerned, the intrinsic and extrinsic diffusion of In in Ge mainly yield information about the charge state of In*V* and the reduced diffusion coefficient D_{In}^*.

Modeling of In diffusion also yields the corresponding profiles of In*V* pairs and vacancies. These profiles normalized by the respective thermal equilibrium concentration are illustrated in Fig. 1. The vacancy profile demonstrates that thermal equilibrium is established $(C_V / C_V^{eq} \approx 1)$. The profile of In*V* follows that of substitutional In. This is characteristic for the foreign-atom controlled diffusion mode; that is, the diffusion profile of In mainly reflects the diffusion of In*V* pairs.

C. Temperature dependence

The temperature dependence of the reduced diffusion coefficient D_{In}^* in Ge is illustrated in Fig. 6. The data are accurately described by an Arrhenius equation with an diffusion activation enthalpy of $Q = (3.51 \pm 0.06)$ eV and a pre-exponential factor $D_o = (5123^{+5142}_{-2566})\ \mathrm{cm}^2\ \mathrm{s}^{-1}$. Earlier data on In diffusion in Ge reported by Dorner *et al.*[20] are shown for comparison. Within the experimental accuracy of this and the former work, the In diffusion coefficients are equal (not shown). In addition, our work confirms the Arrhenius parameter reported by Dorner *et al.*[20] However, these authors have not differentiated between intrinsic and extrinsic diffusion. The close agreement between the former effective In diffusion coefficients and our results for D_{In}^* confirms that the doping level established in the work of Dorner *et al.* was close to intrinsic.

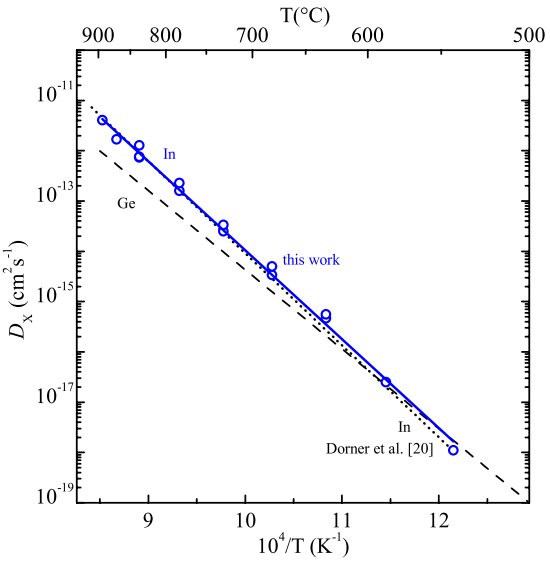

FIG. 6. (Color online) Intrinsic diffusion coefficients D_{In} of indium in Ge (symbol) vs the inverse temperature. The temperature dependence is accurately reproduced by an Arrhenius equation with a diffusion activation enthalpy of $Q = (3.51 \pm 0.06)$ eV and a pre-exponential factor $D_o = (5123^{+5142}_{-2566})\ \mathrm{cm}^2\ \mathrm{s}^{-1}$ (solid line). The dotted line shows results for In diffusion under intrinsic conditions reported by Dorner *et al.* (Ref. 20). For comparison the temperature dependence of Ge self-diffusion (Ref. 22) is also shown (long dashed line).

V. DISCUSSION

The activation enthalpy of 3.51 eV clearly exceeds the value of 2.79 eV predicted recently for In diffusion in Ge via a *V*-mediated ring mechanism.[23,24] The deviation between the experimental result and the theoretical prediction may indicate that In diffusion in Ge is not mediated by the vacancy ring mechanism or that the relationship used in Ref. 23 to calculate the activation enthalpy of dopant diffusion via the *V*-mediated ring mechanism fails for In. The activation enthalpy of Al and Ga diffusion reported by Dorner *et al.*,[17,20] Södervall *et al.*,[18] and Riihimäki *et al.*[19] also clearly exceeds the value predicted for a *V*-mediated ring mechanism. For all three acceptor dopants, the theory predicts positive binding energies of the acceptor to a third nearest neighbor vacancy which indicates a repulsive rather than attractive interaction between the dopant and the vacancy. Therefore, the diffusion activation enthalpy predicted in Ref. 23 is likely too low since the vacancy has to overcome this barrier at third nearest neighbor site in order to promote the diffusion of In. Accordingly, the diffusion of In and of Al and Ga via the vacancy ring mechanism may be hindered since the va-

cancy moving from second to third nearest neighbor site has a high probability to leave the sphere of the dopant. In addition, DFT calculations very likely underestimate the interaction between the acceptor and the vacancy because Ge is predicted to be metallic with zero band gap.[33] Experiments clearly demonstrate that under intrinsic conditions the acceptor is single negative and the vacancy is doubly negatively charged. However, in the DFT calculations of Chroneos *et al.*,[23] the vacancy can only be neutral. This deficiency of DFT calculations to consider charged defects in Ge results in too low values for the migration enthalpy of impurity-vacancy pairs.[33] More precise calculations are expected to provide activation enthalpies of In, Ga, and Al diffusion in Ge that exceed the activation enthalpy of self-diffusion in qualitative agreement with the experimental results as has been shown for Ge self-diffusion using a hybrid functional with exact exchange.[33]

Recently Decoster *et al.*[42] applied the emission channeling technique to In-implanted Ge samples. They found experimental evidence that directly after implantation, a fraction of In atoms occupies the bond-centered (BC) site. In this configuration, the In atom is at the bond center position with two half vacancies or semivacancies on the neighboring sites. Indium in this split-vacancy configuration has been also predicted by Höhler *et al.*[43] to be more stable than an In atom in a full-vacancy configuration. However, according to the results of Decoster *et al.*,[42] the BC configuration disappears completely at 300 °C. Hence for typical diffusion studies with temperatures above 300 °C, it is very unlikely that In in the split-vacancy configuration is more important than In in a full-vacancy configuration.

Recently, Riihimäki *et al.*[19] performed experiments on Ga diffusion in Ge and also observed a concentration independent diffusion. Accordingly, the mobile Ga-*V* complex is singly negatively charged. Small differences in the extrinsic and intrinsic diffusion of Ga like those discussed in this work were, however, not recognized. The experiments on Ga and In diffusion in Ge clearly reveal that the mobile dopant-vacancy complex must be singly negatively charged. It is very likely that Al in Ge behaves similar.

Finally, the impact of implantation damage on dopant diffusion in Ge should be discussed. It has been demonstrated that dopant implantation into crystalline and preamorphized Ge (Refs. 10 and 44–46) and subsequent annealing did not cause any significant enhanced dopant diffusion. This is attributed to the fact that seemingly no end-of-range (EOR) defects are formed after the solid phase epitaxial regrowth (SPER).[10,45,46] Recently, however, Koffel *et al.*[47] provided first direct evidence of EOR defects after SPER of an amorphous Ge layer created by ion implantation. The density and size of the defects strongly depend on temperature and are hardly detectable after annealing at 600 °C. The evolution of EOR defects in Ge is expected to affect dopant diffusion. The extended tails of the In profiles observed after annealing the high-dose implanted Ge sample at 650 °C and the low-dose implanted sample at 550 °C (see Fig. 3) could indicate an enhanced diffusion during the onset of the diffusion annealing. Additional diffusion experiments are presently underway to verify the enhanced diffusion and structural investigations by means of high resolution transmission electron microscopy will help to determine the physical origin.

VI. CONCLUSIONS

The intrinsic and extrinsic diffusion of In in Ge demonstrate that the defect mediating In diffusion is singly negatively charged. The equality in the charge state of the mobile In-vacancy complex and the substitutional dopant causes a factor of 2 differences between In diffusion under intrinsic and extrinsic doping. An activation enthalpy of 3.51 eV was determined for In diffusion that confirms earlier results of Dorner *et al.*[20] The value clearly exceeds the activation enthalpy of 3.13 eV for self-diffusion and is at variance with recent theoretical predictions on the diffusion activation enthalpy of acceptor dopants in Ge that are based on a vacancy-mediated ring mechanism.[23] The equation used in Ref. 23 to predict the activation enthalpy should consider the interaction of the dopants to vacancies on the second and third nearest neighbor sites that in the case of Al, Ga, and In suggests to be repulsive.

ACKNOWLEDGMENTS

This work was supported by the Deutsche Forschungsgemeinschaft under Contract No. BR 1520/6-2.

[1] S. M. Sze, *Physics of Semiconductor Devices* (Wiley, New York, 2001).
[2] G. Nicholas, B. De Jaeger, D. P. Brunco, P. Zimmerman, G. Eneman, K. Martens, M. Meuris, and M. M. Heyns, IEEE Trans. Electron Devices **54**, 2503 (2007).
[3] D. P. Brunco, B. De Jaeger, G. Eneman, J. Mitard, G. Hellings, A. Satta, V. Terzieva, L. Souriau, F. E. Leys, G. Pourtois, M. Houssa, G. Winderickx, E. Vrancken, S. Sioncke, K. Opsomer, G. Nicholas, M. Caymax, A. Stesmans, J. Van Steenbergen, P. W. Mertens, M. Meuris, and M. M. Heyns, J. Electrochem. Soc. **155**, H552 (2008).
[4] A. Satta, E. Simoen, R. Duffy, T. Janssens, T. Clarysse, A. Benedetti, M. Meuris, and W. Vandervorst, Appl. Phys. Lett. **88**, 162118 (2006).
[5] H. Bracht and S. Brotzmann, Mater. Sci. Semicond. Process. **9**, 471 (2006).
[6] S. Brotzmann and H. Bracht, J. Appl. Phys. **103**, 033508 (2008).
[7] S. Brotzmann, H. Bracht, J. Lundsgaard Hansen, A. Nylandsted Larsen, E. Simoen, E. E. Haller, J. S. Christensen, and P. Werner, Phys. Rev. B **77**, 235207 (2008).
[8] H. Bracht, Phys. Rev. B **75**, 035210 (2007).
[9] S. Uppal, A. F. W. Willoughby, J. M. Bonar, N. E. B. Cowern, T. Grasby, R. J. H. Morris, and M. G. Dowsett, J. Appl. Phys. **96**, 1376 (2004).
[10] A. Satta, E. Simoen, T. Clarysse, T. Janssens, A. Benedetti, B. De Jaeger, M. Meuris, and W. Vandervorst, Appl. Phys. Lett. **87**, 172109 (2005).
[11] G. Impellizzeri, S. Mirabella, E. Bruno, A. M. Piro, and M. G. Grimaldi, J. Appl. Phys. **105**, 063533 (2009).
[12] A. Chroneos, B. P. Uberuaga, and R. W. Grimes, J. Appl. Phys. **102**, 083707 (2007).
[13] M. Dionízio Moreira, R. H. Miwa, and P. Venezuela, Phys. Rev. B **70**, 115215 (2004).
[14] K. Sueoka and J. Vanhellemont, Mater. Sci. Semicond. Process. **9**, 494 (2006).
[15] J. Vanhellemont, P. Śpiewak, and K. Sueoka, J. Appl. Phys. **101**, 036103 (2007).
[16] A. Carvalho, R. Jones, C. Janke, J. P. Goss, P. R. Briddon, J. Coutinho, and S. Öberg, Phys. Rev. Lett. **99**, 175502 (2007).
[17] P. Dorner, W. Gust, A. Lodding, H. Odelius, B. Predel, and U. Roll, Acta Metall. **30**, 941 (1982).
[18] U. Södervall, H. Odelius, A. Lodding, U. Roll, B. Predel, and W. Gust, and P. Dorner, Philos. Mag. A **54**, 539 (1986).
[19] I. Riihimäki, A. Virtanen, S. Rinta-Anttila, P. Pusa, J. Räisänen, and The ISOLDE Collaboration, Appl. Phys. Lett. **91**, 091922 (2007).
[20] P. Dorner, W. Gust, A. Lodding, H. Odelius, B. Predel, and U. Roll, Z.

Metallkd. **73**, 325 (1982).
[21]M. Werner, H. Mehrer, and H. D. Hochheimer, Phys. Rev. B **32**, 3930 (1985).
[22]E. Hüger, U. Tietze, D. Lott, H. Bracht, D. Bougeard, E. E. Haller, and H. Schmidt, Appl. Phys. Lett. **93**, 162104 (2008).
[23]A. Chroneos, H. Bracht, R. W. Grimes, and B. P. Uberuaga, Appl. Phys. Lett. **92**, 172103 (2008).
[24]The value given in Table I of Ref. 23 for the migration enthalpy of the In-vacany cluster is actually 1.35 eV. With this value, an activation enthalpy of 2.79 eV for In diffusion in Ge is predicted.
[25]D. B. Cuttriss, Bell Syst. Tech. J. **40**, 509 (1961).
[26]A. Chroneos, R. Kube, H. Bracht, R. W. Grimes, and U. Schwingenschlögl (submitted).
[27]H. Bracht, Mater. Sci. Semicond. Process. **7**, 113 (2004).
[28]H. Bracht, N. A. Stolwijk, and H. Mehrer, Phys. Rev. B **43**, 14465 (1991).
[29]A. Chroneos, R. W. Grimes, B. P. Uberuaga, S. Brotzmann, and H. Bracht, Appl. Phys. Lett. **91**, 192106 (2007).
[30]J. Coutinho, C. Janke, A. Carvalho, S. Öberg, V. J. B. Torres, R. Jones, and P. R. Briddon, Defect Diffus. Forum **273–276**, 93 (2008).
[31]A. Fazzio, A. Janotti, and J. R. Antonio da Silva, and R. Mota, Phys. Rev. B **61**, R2401 (2000).
[32]A. Chroneos, R. W. Grimes, B. P. Uberuaga, and H. Bracht, Phys. Rev. B **77**, 235208 (2008).
[33]B. P. Uberuaga, G. Henkelman, H. Jónsson, S. T. Dunham, W. Windl, and R. Stumpf, Phys. Status Solidi B **233**, 24 (2002).
[34]M. Naganawa, Y. Shimizu, M. Uematsu, K. M. Itoh, K. Sawano, Y. Shiraki, and E. E. Haller, Appl. Phys. Lett. **93**, 191905 (2008).
[35]K. Björkqvist, B. Domeij, L. Eriksson, G. Fladda, A. Fontell, and J. W. Mayer, Appl. Phys. Lett. **13**, 379 (1968).
[36]K. Björkqvist, D. Sigurd, G. Fladda, and G. Bjarnholt, Radiat. Eff. **6**, 141 (1970).
[37]U. Feuser, R. Vianden, and A. F. Pasquevich, Hyperfine Interact. **60**, 829 (1990).
[38]U. Feuser, R. Vianden, E. Alves, M. F. da Silva, E. Szilágyi, F. Pászti, and J. C. Soares, Nucl. Instrum. Methods Phys. Res. B **59–60**, 1049 (1991).
[39]H. Häßlein, R. Sielemann, M. Brüßler, and H. Metzner, Hyperfine Interact. **84**, 65 (1994).
[40]H. Haesslein, R. Sielemann, and C. Zistl, Phys. Rev. Lett. **80**, 2626 (1998).
[41]C. J. Glover, A. P. Byrne, and M. C. Ridgway, Nucl. Instrum. Methods Phys. Res. B **175–177**, 51 (2001).
[42]S. Decoster, B. De Vries, U. Wahl, J. G. Correia, and A. Vantomme, J. Appl. Phys. **105**, 083522 (2009).
[43]H. Höhler, N. Atodiresei, K. Schroeder, R. Zeller, and P. H. Dederichs, Phys. Rev. B **71**, 035212 (2005).
[44]C. Wündisch, M. Posselt, W. Anwand, B. Schmidt, A. Mücklich, and W. Skorupa, Proceedings of the 16th IEEE International Conference on Advanced Thermal Processing of Semiconductors, RTP 2008, Las Vegas, NV, 2008 (unpublished).
[45]A. Satta, E. Simoen, T. Janssens, T. Clarysse, B. De Jaeger, A. Benedetti, I. Hoflijk, B. Brijs, M. Meuris, and W. Vandervorst, J. Electrochem. Soc. **153**, G229 (2006).
[46]M. Posselt, B. Schmidt, W. Anwand, R. Grötzschel, V. Heera, A. Mücklich, C. Wündisch, W. Skorupa, H. Hortenbach, S. Gennaro, M. Bersani, D. Giubertoni, A. Möller, and H. Bracht, J. Vac. Sci. Technol. B **26**, 430 (2008).
[47]S. Koffel, N. Cherkashin, F. Houdellier, M. J. Hytch, G. Benassayag, P. Scheiblin, and A. Claverie, J. Appl. Phys. **105**, 126110 (2009).